Korean J. Chem. Eng., 37(12), 2317-2325 (2020)
DOI: 10.1007/s11814-020-0655-6

pISSN: 0256-1115
eISSN: 1975-7220

Thermally stable amine-functionalized silica sorbents using one-pot synthesis method for CO_2 capture at low temperature

Seong Bin Jo*, Ho Jin Chae*, Tae Young Kim, Jeom-In Baek***, Dhanusuraman Ragupathy****, Soo Chool Lee*,†, and Jae Chang Kim**,†**

*Research Institute of Advanced Energy Technology, Kyungpook National University, Daegu 41566, Korea
**Department of Chemical Engineering, Kyungpook National University, Daegu 41566, Korea
***Korea Electric Power Research Institute, Daejeon 34056, Korea
****Department of Chemistry, National Institute of Technology Puducherry, Karaikal 609609, India
(*Received 18 June 2020 • Revised 4 August 2020 • Accepted 4 August 2020*)

Abstract−Amine-functionalized silica sorbents have been widely investigated for post-combustion CO_2 capture at low temperature. In previous studies, amine-functionalized silica sorbents were prepared using a synthetic hierarchically porous silica, which is not commercially available in large quantities, because porous silica support structures strongly influence CO_2 capture performance. Here, we propose a feasible and facile fabrication method for amine-functionalized silica sorbents using 3-aminopropyltrimethoxy silane (APTS) and fumed silica (FS), where APTS serves as both an active material and a binder. The APTS-functionalized FS sorbents have large amounts of active amino groups and porous structures and demonstrate good multicycle stability with excellent CO_2 capture performance. In addition, cetyltrimethylammonium bromide was found to improve the diffusion pathway of CO_2, leading to enhanced CO_2 capture capacity because of the suppression of excessive condensation during preparation. Therefore, the APTS-functionalized FS sorbents could be cost- and energy-efficiently prepared using a novel one-pot synthesis method; the resulting sorbents exhibit excellent CO_2 capture performance.

Keywords: CO_2 Capture Sorbents, One-pot Synthesis, 3-Aminopropyltrimethoxy-silane (APTS), Porous Structures, Thermal Stability

INTRODUCTION

The current anthropogenic climate emergency is a major challenge facing humanity. Climate change continues to accelerate because of increasing concentrations of greenhouse gases such as CO_2, CO, SO_2, and NO_x in the atmosphere. In particular, CO_2 greatly contributes to global warming because of its high concentration resulting from the combustion of fossil fuels (oil, natural gas, and coal) [1-3]. The effects of global climate change are already being observed worldwide and are expected to increase substantially throughout this century and beyond [4-6]. Rising atmospheric CO_2 concentration, higher temperatures, and altered precipitation patterns are leading to natural disasters (e.g., drought, wildfires, air pollution, sea level rise, coastal flooding, ocean acidification, intense storms, etc.) and disrupted ecosystems and are even affecting human health [7-10]. Over the past decade, numerous methods to capture CO_2 from coal-fired power plants, which are a major source of CO_2 emissions, have been investigated, including membrane separation, absorption with a solvent, and adsorption using molecular sieves [11-24]. Successful control of CO_2 relies on the development of cost-effective methods to capture CO_2 from flue gas emitted from coal-fired power plants. Amine-functionalized solid sorbents are promising candidates for capturing CO_2. In a manner similar to liquid amine scrubbing systems, amino groups in amine-based solid sorbents react with CO_2 reversibly.

In previous studies, two methods have been used to prepare amine-functionalized solid sorbents for capturing CO_2: impregnation and grafting. Amino groups are physically introduced into hierarchically porous silica supports such as MCM-41, SBA-15, and KIT-6 in the impregnation method [25-30], whereas the amine is covalently tethered to the surface of the porous silica support in amine-grafted sorbents [28,31-37]. Although amine-impregnated sorbents have remarkable CO_2 capture capacity, this capacity dramatically decreases during multiple CO_2 capture cycles. This phenomenon results from amine leaching and degradation during the regeneration process at high temperatures [26]. Although amine-grafted sorbents are thermally stable, they exhibit a relatively low CO_2 capture capacity compared with amine-impregnated sorbents [38,39]. Moreover, mesoporous silica is presently not commercially available in large quantities. Thus, Choi et al. developed a highly scalable synthesis of functionalized-Polyethylenimine (PEI)/silica sorbents using a porous silica synthesized by spray-drying a water slurry containing 10 wt% fumed silica (FS) and 0.5 wt% silica sol as a binder to form a porous structure in a silica support; these sorbents exhibited a large CO_2 working capacity and good long-term stability [40].

In the present study, amine-functionalized FS sorbents were developed in large quantities without synthesizing hierarchically porous

†To whom correspondence should be addressed.
E-mail: soochool@knu.ac.kr, kjchang@knu.ac.kr

silica supports. In this process, 3-aminopropyltrimethoxy silane (APTS) serves as both an active material and a binder, whereas FS is used as a support material. In addition, the effect of the surfactant was also elucidated to improve the CO_2 capture performance. The properties of the sorbents were investigated using Fourier transform infrared spectroscopy (FTIR), Brunauer-Emmett-Teller (BET) analysis, ultra-high-resolution field-emission scanning electron microscopy (UHR-FE-SEM), thermogravimetric analysis (TGA), and elemental analysis (EA). The CO_2 capture capacity of the sorbents was investigated during multiple cycles in the presence of 1 vol% CO_2 and 10 vol% H_2O in a fixed-bed reactor.

EXPERIMENTAL

1. Preparation of Sorbents

To synthesize amine-functionalized sorbents, APTS (Sigma-Aldrich) and industrial FS (Aerosil 200) were chosen as the active material and support material, respectively. First, FS was added to a three-necked round-bottom flask containing anhydrous ethanol as a solvent. The solution was stirred vigorously at room temperature until the FS suspension was well distributed. Next, 1 mL of distilled water was added to the mixture, which was stirred for another 30 min. The temperature was rapidly increased to 70 °C and APTS was grafted onto the surface of FS corresponding to the grafting. The resulting mixture was stirred and refluxed continuously for 24 h. The mixture was dried in a rotary evaporator at 40-60 °C and dried overnight in a furnace under N_2 at 100 °C. In this procedure, the sorbent was not filtered or washed before drying; therefore, all of the solvents (anhydrous ethanol and water) were removed by evaporation during the drying of sorbent at 100 °C [41]. The resulting amine-functionalized FS sorbents are denoted as FS-APTS*x*, where *x* represents the weight percent of APTS.

2. Characterization

The characteristic functionality of amine-functionalized FS sorbents was determined by FTIR analysis. The samples were first ground and subsequently diluted with KBr, and the spectra were recorded in the range 4,000-400 cm^{-1}. N_2 adsorption-desorption isotherms at −196 °C were measured using a Micromeritics ASAP 2020 instrument to characterize the textural properties of the materials. The FS was degassed at 300 °C for 6 h under high vacuum before analysis, whereas the amine-functionalized FS sorbents were degassed at 100 °C to prevent amine vaporization. In addition, UHR-FE-SEM (Hitachi, S-4800) was performed at the Korea Basic Science Institute in Daegu to identify the crystalline phase and morphology of the samples. TGA was used to investigate the thermal stability of the amine-functionalized FS sorbents. TGA was performed from room temperature to 700 °C at a heating rate of 5 °C/min in a highly pure N_2 atmosphere with a flow rate of 50 mL/min. The N content in the sorbents was analyzed by EA.

3. Adsorption and Regeneration Tests

The CO_2 sorption and desorption processes were determined by monitoring the CO_2 concentration using gas chromatography (GC). The sorbent (0.5 g) was packed into a fixed-bed reactor with a diameter of 1 cm, and the reactor was placed in an electric furnace at atmospheric pressure. To prevent the condensation of water vapor, the inlet and outlet lines of the reactor were maintained at temperatures greater than 100 °C using heating tape before the injection of gas into the reactor and GC column. A 1/8-inch stainless steel tube packed with Porapak Q was used as the column. The outlet gases from the reactor were analyzed automatically every 4 min using a thermal conductivity detector (TCD, Donam Systems Inc.) equipped with an auto sampler (Valco Instruments Co. Inc.). First, the feed gas (1 vol% CO_2, balance N_2, 40 mL/min) was passed through the bed at the sorption temperature of 60 °C. When the CO_2 concentration of the outlet gas reached the concentration of the inlet CO_2 feed gas (1 vol%) in the sorption process, the gas composition was changed from the feed gas to pure N_2 to purge the CO_2 gas from the reactor. After the concentration of CO_2 decreased to zero, the temperature was increased to 120 °C to regenerate the spent sorbents.

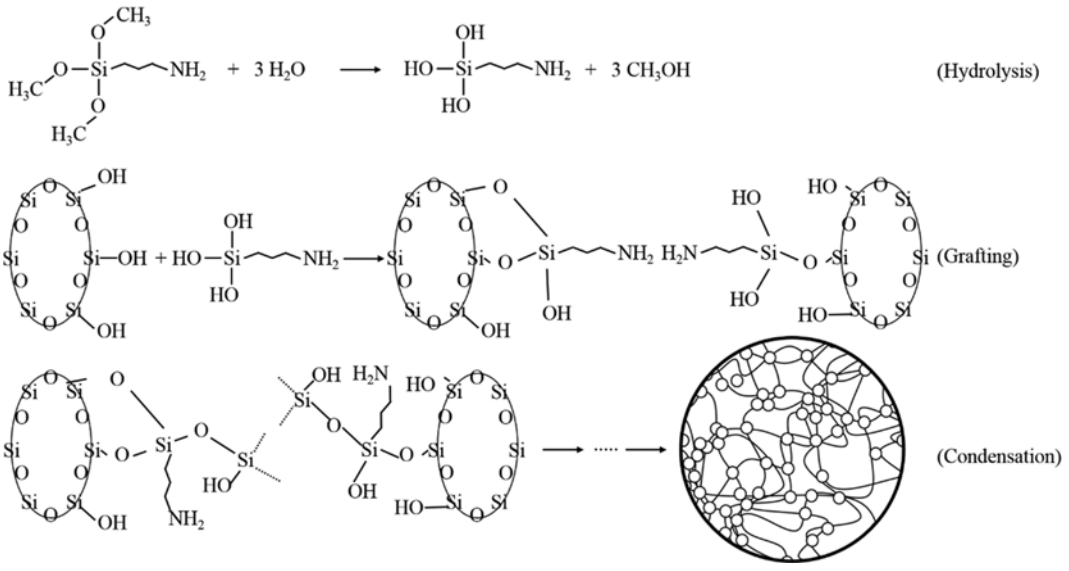

Fig. 1. Schematic of the one-pot synthesis method for APTS-functionalized fumed silica sorbents.

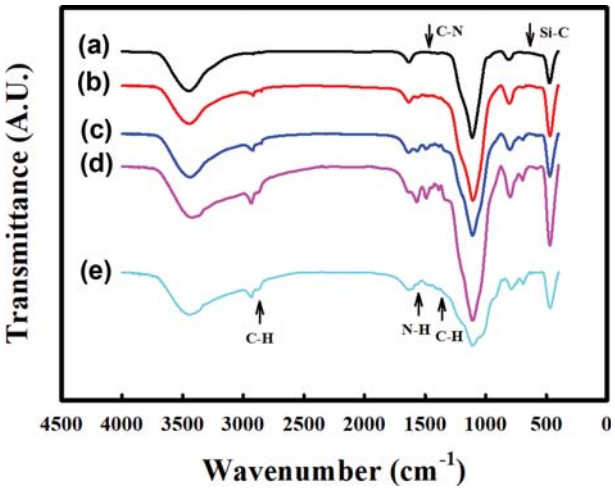

Fig. 2. FTIR spectra of (a) bare-fumed silica, (b) FS-APTS40, (c) FS-APTS50, (d) FS-APTS60, and (e) FS-APTS70 sorbents.

RESULTS AND DISCUSSION

Fig. 1 shows a schematic of the facile fabrication of APTS-functionalized FS sorbents using a one-pot synthesis method, which consisted of three steps: (1) hydrolysis, (2) grafting, and (3) condensation. First, APTS was hydrolyzed with H_2O, forming $Si(OH)_3(CH_2)_3NH_2$ and methanol. The produced amino silane ($Si(OH)_3(CH_2)_3NH_2$) was grafted onto the silanol groups in the FS. Then, an excess molar amount of $Si(OH)_3(CH_2)_3NH_2$ was interlinked between the grafted amino silane on the surface of the FS. In this proposed facile fabrication of APTS-functionalized FS sorbents, APTS functions as both an active material and a binder.

Fig. 2 shows the FTIR spectra collected to reveal the functional groups and chemical bonds of the bare FS and amine-functionalized FS sorbents. As evident in Fig. 2, the spectrum of FS shows peaks at 3,445, 1,635, 1,200-1,100, 810, and 475 cm^{-1}. The bands at 3,445, 1,635, and 810 cm^{-1} are attributed to the stretching and bending vibrations of silanol groups (Si-OH) on the silica surface and to physisorbed water [41]. The intense bands at 1,200-1,100 and 475 cm^{-1} correspond to the asymmetric stretching and bending of siloxane groups (Si-O-Si) [42]. Accordingly, the spectral features of FS remained intact after the amine modification. In the spectra of all of the amine-functionalized FS sorbents, vibrations at 3,350 and 1,616 cm^{-1} were caused by stretching and bending of N-H bonds, whereas the peaks at 2,950-2,850, 1,490, and 1,410 cm^{-1} are attributed to vibrations of C-H bonds in APTS [41,42]. The vibration at 695 cm^{-1} and the small shoulder at 1,600-1,300 cm^{-1} are assigned to Si-C and C-N bonds, respectively. The emergence of new peaks attributed to C-H, N-H, Si-C, and C-N bonds is consistent the existence of APTS in the sorbent [41].

Table 1 lists the EA results of amine-functionalized FS sorbents. As listed in Table 1, the N content increases from 2.38 to 6.58 wt% with increasing APTS loading. The O content initially increases with increasing APTS loading, reaching a maximum O content of 4.67 wt% at an APTS loading of 50 wt%, and then decreases at higher APTS loadings. This result might be due to the fact that the number of silanol groups (Si-OH) increases with increasing APTS loading until the APTS loading reaches 50 wt%, and the decrease in O content at higher APTS loadings is attributed to excess condensation between APTS and silanol groups.

Table 1. Elemental analysis results for amine-functionalized fumed silica sorbents

Sample	N (wt%)	C (wt%)	H (wt%)	O (wt%)
FS-APTS40	2.38	6.71	1.55	2.91
FS-APTS50	4.63	14.75	3.20	4.67
FS-APTS60	4.91	13.55	2.97	4.09
FS-APTS70	6.58	17.53	4.45	3.85

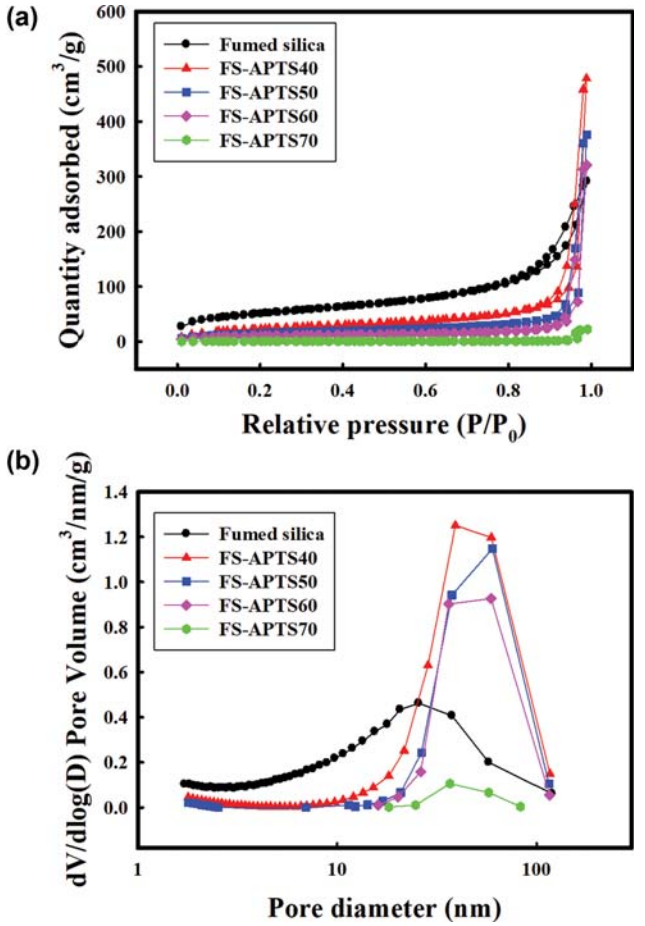

Fig. 3. (a) Nitrogen adsorption-desorption isotherms and (b) pore size distribution of bare fumed silica and amine-functionalized sorbents.

Fig. 3 shows the N_2 adsorption-desorption isotherms of the bare FS and amine-functionalized FS sorbents. As shown in Fig. 3(a), the bare FS and APTS-functionalized FS all exhibit pseudo-Type II isotherms. Pseudo-Type II isotherms have adsorption hysteresis at high P/P_0, characteristic of nonporous or macroporous materials [43]. The volume of adsorbed N_2 decreases with increasing amine loading. However, the amine-functionalized FS sorbent shows a greater volume of adsorbed N_2 than the bare FS, with the exception of the FS-APTS70 sorbent. Fig. 3(b) shows the pore size distribution of bare FS and amine-functionalized FS sorbents

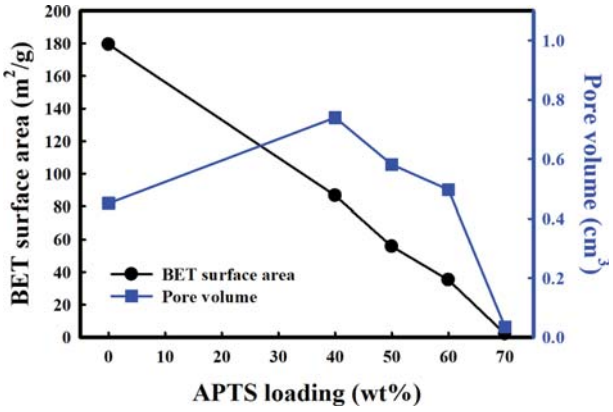

Fig. 4. Variation in the BET surface area and pore volume of amine-functionalized sorbents as a function of the APTS amount.

measured using the Barrett-Joyner-Halenda (BJH) method. The bare FS exhibited a broad pore size distribution. By contrast, the amine-functionalized FS showed a relatively well-defined pore size distribution from 10 to 100 nm, except for the FS-APTS70 sorbent. In the case of the FS-APTS70 sorbent, the pores were filled with APTS molecules.

To convey the surface properties of the amine-functionalized FS sorbents prepared by the one-pot synthesis method in detail, the variation in the BET surface area and pore volume as a function of APTS loading are described in Fig. 4. As evident in Fig. 4 and Table 2, the BET surface areas of the sorbents abruptly decreased with increasing APTS loading. The BET surface area of the FS decreased from 179.4 to 2.1 m^2/g as the APTS loading was increased from 0 to 70 wt%, because micropores of fumed silica were filled with APTS materials. The pore volume of amine-functionalized FS sorbents initially increased at 40 wt% APTS loading and then decreased as the APTS loading was increased due to the formation of additional pore structure (10-100 nm). As listed in Table 2, the average pore size increased with increasing APTS loading because APTS molecules percolated into the micropores, causing an increase in the average pore size. The size of the bare FS was 33.5 nm, and that of amine-functionalized FS sorbents FS-APTS*x* (*x*=40, 50, 60, 70) was 69.3, 107.7, 170.6, and 2,835.4 nm, respectively. Thus, the nanoparticle size increased with increasing APTS loading, especially for the FS-APTS70 sorbent. We suspect that the surface of the FS was bound to silanol groups in APTS molecules and coated with APTS molecules. For the amine-functionalized FS sorbents, the increasing pore volume, BET isotherms, and pore size distribution indicate that porous structures were formed through the one-pot synthesis method. We speculated that the FS-APTS70 sorbent would exhibit poor CO_2 capture performance because of its low BET surface area and small pore volume, indicating overloading of APTS molecules on the surface of the FS. The BET results show that a pore structure was formed via the one-pot synthesis method.

Fig. 5 shows SEM images of FS and amine-functionalized FS sorbents. The image of bare FS shows agglomerates of uniformly sized nanoparticles with a diameter of approximately 40 nm. For the FS-APTS40 sorbent, APTS appears to be coated onto the surface of the FS. The diameter of the nanoparticles of the amine-functionalized FS increased with increasing APTS loading until the APTS loading reached 50 wt%; the nanoparticles were interconnected by APTS molecules at higher APTS loadings, corresponding to the nanoparticle sizes listed in Table 2. These SEM images show that the APTS concentration played a major role in the extent of binding between nanoparticles of FS. This phenomenon is attributed to the self-assembled APTS molecules and the condensation of grafted-silanol groups between surfaces on FS. For the FS-APTS70 sorbent, however, the space between FS was fully covered with APTS molecules during amine modification. These results correspond to textural properties such as the BET surface area, pore volume, and the nanoparticle size, as shown in Fig. 4 and Table 2.

To investigate the thermal stability of the amine-functionalized FS sorbents, we subjected them to TGA. TGA was performed from room temperature to 700 °C at a heating rate of 5 °C/min with the samples under a pure N_2 atmosphere flowing at 50 mL/min. TGA results of amine-functionalized FS sorbents are depicted in Fig. 6 where, as shown, the amine-functionalized FS sorbents showed weight-loss peaks after approximately 300 °C, suggesting decomposition of loaded APTS. All amine-functionalized FS sorbents remained stable below 300 °C, suitable for sorption (60 °C) and desorption (120 °C) processes. The weight loss of FS-APTS40, FS-APTS50, FS-APTS60, and FS-APTS70 sorbents was 16, 21, 24, and 23%, respectively. However, these weight loss values did not correspond to the quantity of APTS added in the synthesis step due to the weight change during hydrolysis, grafting, and condensation, as mentioned in Fig. 1.

Fig. 7 shows the CO_2 capture performance of FS-APTS*x* (*x*= 40, 50, 60, 70) sorbents with the sorption performed at 60 °C under dry conditions (1 vol% CO_2, N_2 balance). The CO_2 capture capacity was calculated from the breakthrough curves. In principle, the CO_2 capture capacity should increase with increasing APTS load-

Table 2. Textural properties of bare fumed silica and amine-functionalized sorbents

Sample	BET surface area (m^2/g)	Pore volume (cm^3/g)	Average pore size (nm)	Nanoparticle size (nm)
Fumed silica	179.4	0.45	11.7	33.5
FS-APTS40	86.6	0.74	35.3	69.3
FS-APTS50	55.7	0.58	43.7	107.7
FS-APTS60	35.2	0.50	45.7	170.6
FS-APTS70	2.1	0.03	40.3	2,835.4

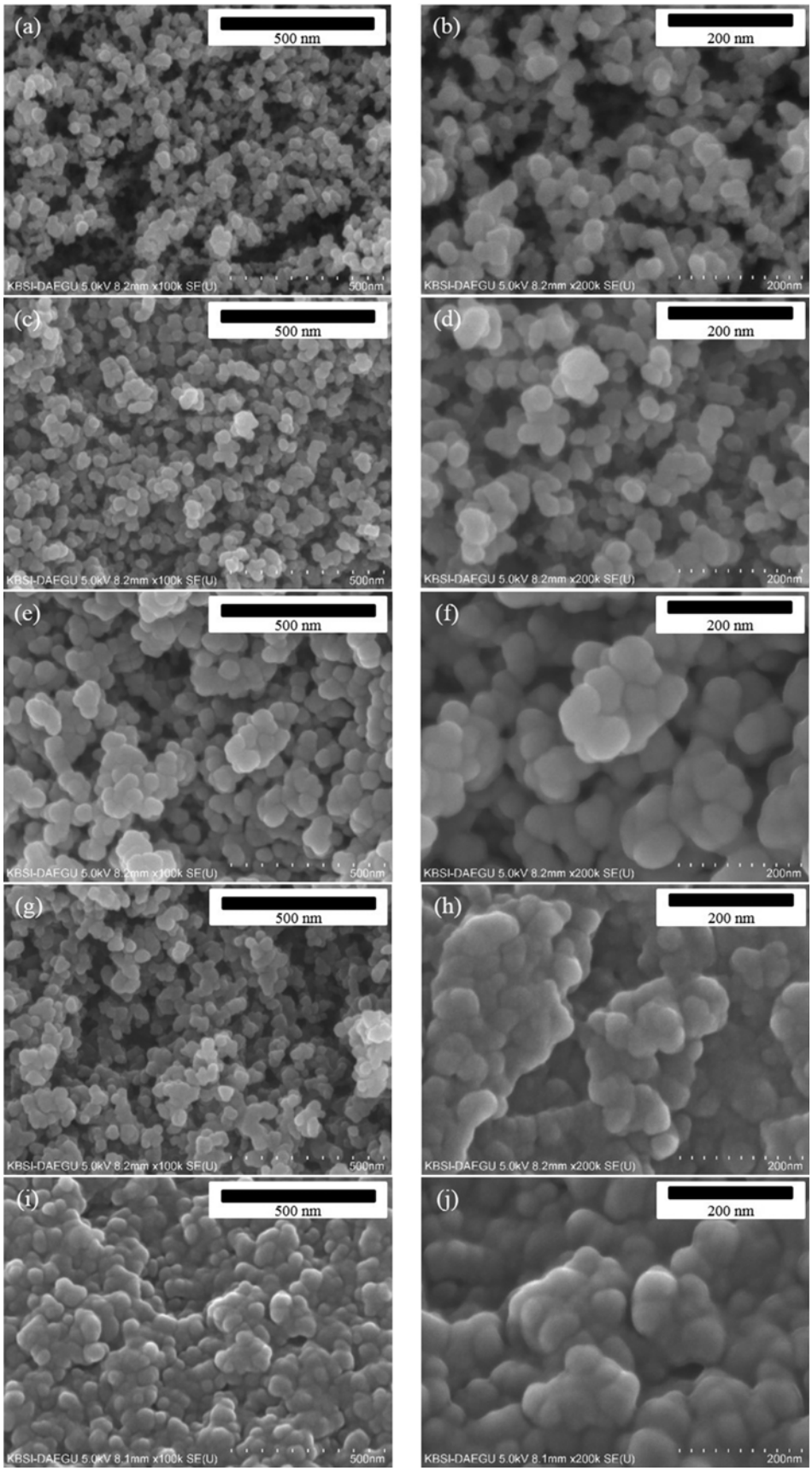

Fig. 5. SEM image of ((a) and (b)) bare-fumed silica, ((c) and (d)) FS-APTS40, ((e) and (f)) FS-APTS50, ((g) and (h)) FS-APTS60, and ((i) and (j)) FS-APTS70 sorbents.

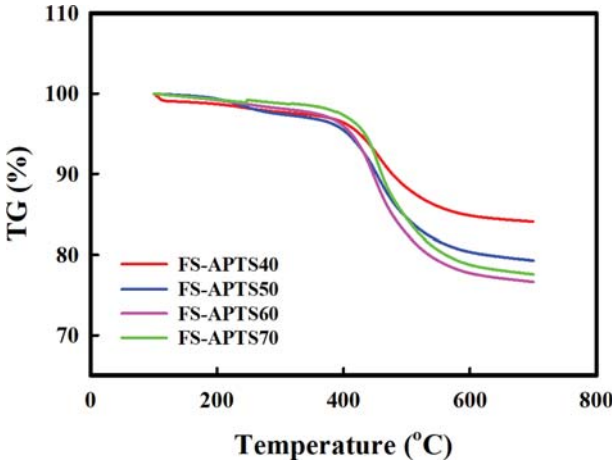

Fig. 6. TGA results for amine-functionalized sorbents in the temperature range from 100 to 700 °C.

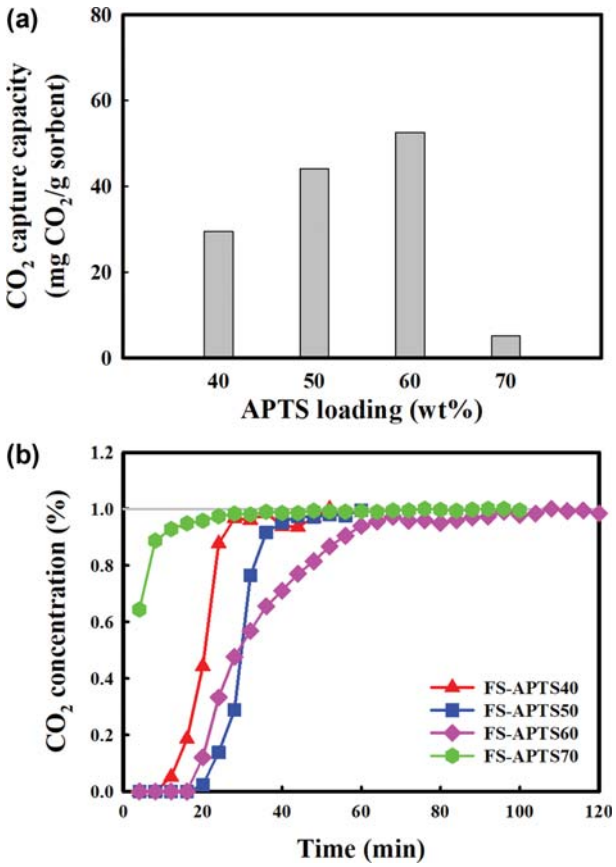

Fig. 7. (a) CO_2 capture capacity and (b) breakthrough curves of FS-APTS40, FS-APTS50, FS-APTS60, and FS-APTS70 in the presence of 1 vol% CO_2 at 60 °C.

ing. The CO_2 capture capacity initially increased from 29.5 to 52.5 mg CO_2/g sorbent, reaching a maximum CO_2 capture capacity at an APTS loading of 60 wt%. For the FS-APTS70 sorbent, however, the CO_2 capture capacity dramatically decreased to 5.1 mg CO_2/g sorbent, as expected. Fig. 7(b) shows the breakthrough curves of the sorbents in the presence of 1 vol% CO_2 at 60 °C. The breakthrough time for the FS-APTS*x* (*x*=40, 50, 60, 70) sorbents was approximately 8, 20, 16, and 0 min, respectively. Although the FS-APTS50 sorbent exhibited a lower CO_2 capture capacity than the FS-APTS60 sorbent, the FS-APTS50 sorbent exhibited the longest breakthrough time and a high slope after the breakthrough point. By contrast, the FS-APTS70 sorbent exhibited a small CO_2 capture capacity and a breakthrough time of zero. These results suggest that the pore structures filled with APTS molecules hindered the diffusion of CO_2 to react with active sites in the pores.

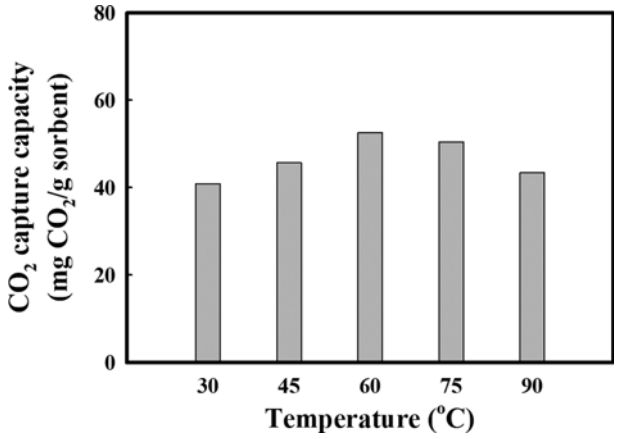

Fig. 8. CO_2 capture capacity of FS-APTS60 sorbents in the presence of 1 vol% CO_2 at different temperatures.

Fig. 8 shows the CO_2 capture capacity as a function of sorption temperature for the FS-APTS60 sorbent at different temperatures ranging from 30 to 90 °C in the presence of 1 vol% CO_2 (N_2 balance). As evident in Fig. 8, the CO_2 capture capacity of the amine-functionalized sorbent initially increased from 40.9 mg CO_2/g sorbent at 30 °C to 51.2 mg CO_2/g sorbent at 60 °C and then decreased to 43.4 mg CO_2/g sorbent at 90 °C. These results are attributed to the slow diffusion of CO_2 to the active amine sites inside amine-functionalized FS sorbent pores at low temperatures because of pore blocking by APTS molecules and to relatively slow reactions of the amine groups with CO_2. These factors led to kinetic limitations, even though lower temperatures are thermodynamically more suitable for CO_2 capture [44]. The kinetic limitation and diffusional resistance diminished as the temperature increased; however, the CO_2 capture capacity decreased at temperatures beyond 75 °C. This behavior indicates that the thermodynamic equilibrium between CO_2 and amine governed CO_2 sorption instead of chemical kinetics. Hence, an increase in sorption temperature beyond 75 °C would have enhanced the kinetic reaction rate but was not favorable in achieving the highest CO_2 capture. Accordingly, the optimal sorption temperature was 60 °C with a CO_2 capture capacity of 51.2 mg CO_2/g sorbent in the presence of 1 vol% CO_2.

To improve CO_2 capture performance, i.e., the CO_2 capture capacity and kinetics, surfactant-promoted sorbents were prepared using the one-pot synthesis method. The principle of surfactant-promoted sorbents is that the surfactant provides an additional pathway for CO_2 to active amine sites and suppresses the condensation between the amino groups on silica supports and the self-assembly of APTS molecules, enhancing the amine efficiency [28]. Three surfactants—

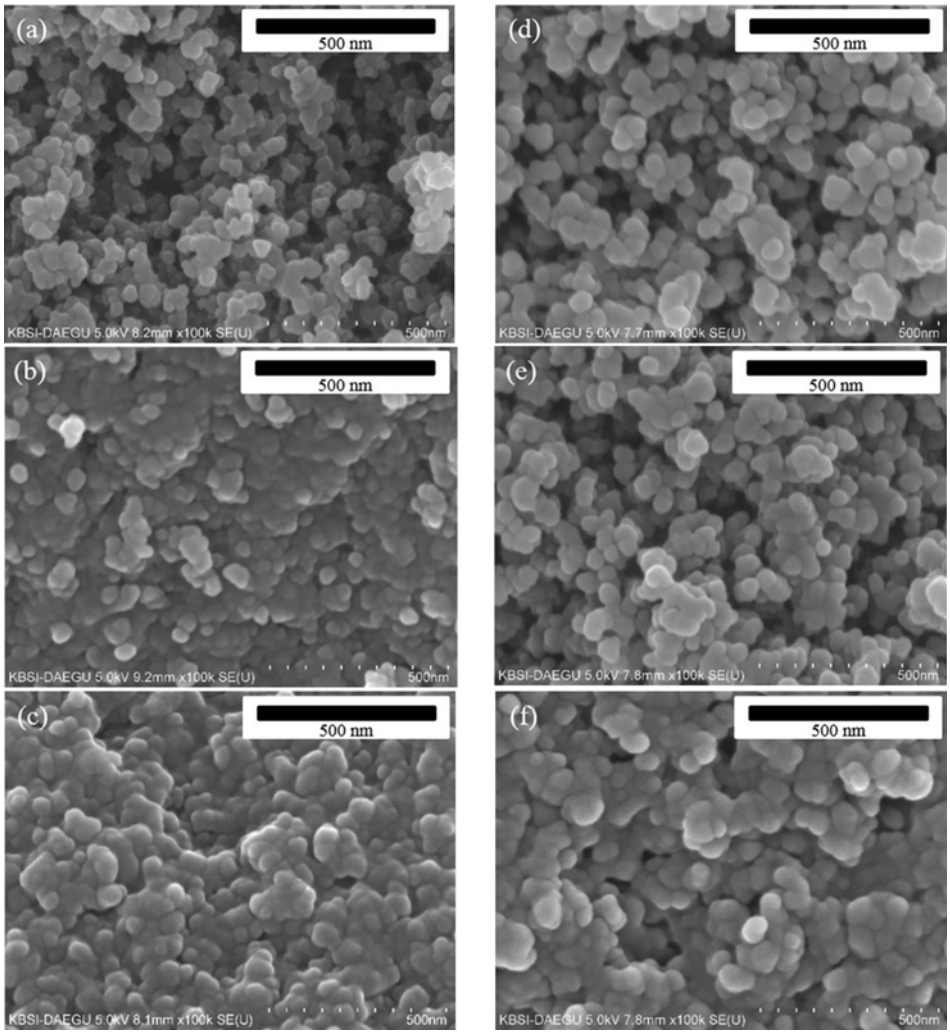

Fig. 9. SEM image of (a) FS-APTS60, (b) FS-APTS65, (c) FS-APTS70, (d) FS-APTS60-CTAB5, (e) FS-APTS65-CTAB5, and (f) FS-APTS70-CTAB5 sorbents.

sodium dodecyl sulfate (SDS), cetyltrimethylammonium bromide (CTAB), and PEO20PPO70PEO20 (Pluronic P123)—were investigated to determine the surfactant that best promotes CO_2 sorption. The CO_2 capture capacity of surfactant-promoted sorbents is shown in Fig. S1, where the surfactant-promoted sorbents contained 60 wt% APTS and 5 wt% of a different surfactant (SDS, CTAB, and P123, respectively). The CO_2 capture capacity of the FS-APTS60 sorbent was 52.5 mg CO_2/g sorbent, whereas that of the surfactant-promoted sorbents was 60.1, 69.9, and 30.7 mg CO_2/g sorbent, respectively. Notably, SDS and CTAB improved the CO_2 capture capacity of the surfactant-promoted sorbents, whereas P123 diminished it. Among the surfactants, CTAB was chosen because it afforded the greatest improvement in CO_2 capture capacity: 33.0%, from 52.5 to 69.9 mg CO_2/g sorbent in the presence of 1 vol% CO_2 at 60 °C.

Fig. 9 shows SEM images of APTS-functionalized FS sorbents with and without CTAB: (a) FS-APTS60, (b) FS-APTS65, (c) FS-APTS70, (d) FS-APTS60-CTAB5, (e) FS-APTS65-CTAB5, and (f) FS-APTS70-CTAB5. As shown in Fig. 9, the agglomeration of the nanoparticles in the sorbents increased with increasing APTS loading. The pore structure of the sorbents without surfactant was overloaded with APTS because of the excess APTS loading amount. In the case of the sorbents with CTAB, however, the pore structure remained the same with increasing APTS loading amount. These SEM images show that the CTAB suppressed the excessive condensation between silanol groups in the sorbents, leading to less agglomeration. Table 3 lists the textural properties of the APTS-functionalized FS sorbents with and without CTAB. For the FS-

Table 3. Textural properties of amine-functionalized fumed silica sorbents with and without CTAB

	BET surface area (m^2/g)	Pore volume (cm^3/g)	Average pore size (nm)
FS-APTS60	35.2	0.50	61.0
FS-APTS60-CTAB5	21.3	0.33	62.5
FS-APTS65	0.28	0.01	43.2
FS-APTS65-CTAB5	21.6	0.28	58.4
FS-APTS70	2.1	0.03	59.0
FS-APTS70-CTAB5	2.9	0.04	60.1

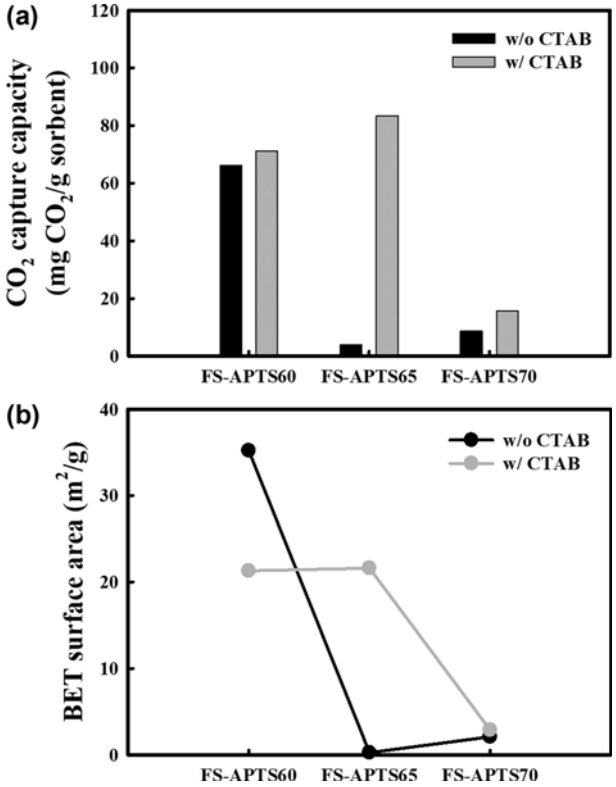

Fig. 10. (a) CO_2 capture capacity and (b) BET surface area of FS-APTS60, FS-APTS65, and FS-APTS70 sorbents with and without 5 wt% CTAB, in the presence of 1 vol% CO_2 and 10 vol% H_2O at 60 °C.

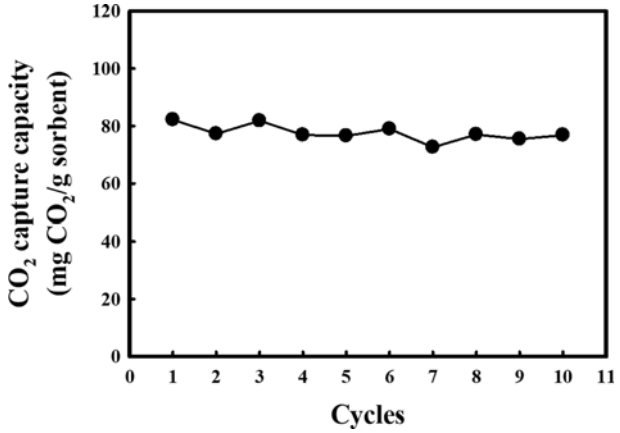

Fig. 11. CO_2 capture capacity of FS-APTS65-CTAB5 over 10 cycles in the presence of 1 vol% CO_2 and 10 vol% H_2O at 60 °C.

APTS60-CTAB5 sorbents, the BET surface area and pore volume decreased after the addition of CTAB. Interestingly, in the case of FS-APTS65-CTAB5, the BET surface area, pore volume, and average pore size were improved by addition of CTAB. For FS-APTS70-CTAB5, however, the textural properties did not change.

Fig. 10 shows the (a) CO_2 capture capacity and (b) BET surface area of APTS-functionalized FS sorbents with and without CTAB. Although the CO_2 capture capacity varied with the APTS loading amount, it increased after introduction of CTAB, as shown in Fig. S2. These results lead to the conclusion that the surfactant suppresses the condensation of the amino groups on the surface of the silica support and provides an additional pathway for CO_2 to the amine site, leading to an increase in the CO_2 capture capacity. Surprisingly, the CO_2 capture capacity of the FS-APTS65-CTAB5 sorbent was 83.4 mg CO_2/g sorbent in humid (1 vol% CO_2 and 10 vol% H_2O) conditions, which is much higher than that of the FS-APTS60-CTAB5 sorbent. These results might be due to a synergetic effect between surfactant and water vapor. In addition, it is found that the trends of the CO_2 capture capacity and the BET surface are similar, as shown in Fig. 10(b).

To investigate the multicycle stability, we investigated the CO_2 capture capacity of the surfactant-promoted sorbent over ten cycles; the results are shown in Fig. 11. The CO_2 sorption and regeneration tests were conducted on FS-APTS65-CTAB5 in the presence of 1 vol% CO_2 and 10 vol% H_2O at sorption (60 °C) and 100 vol% N_2 at regeneration (120 °C). As shown in Fig. 11, the CO_2 capture capacity over ten cycles was 83.4, 77.3, 81.8, 76.9, 76.6, 79.0, 72.6, 77.0, 75.4, and 76.8 mg CO_2/g sorbent, respectively. It is evident that the CO_2 capture capacity of the surfactant-promoted sorbent clearly showed stable CO_2 capture capacity over ten cycles under humid conditions, because of thermally stable structures at a regeneration temperature of 120 °C (Fig. S3).

Therefore, the prepared FS-APTS*x* sorbents contain a relatively large amount of active materials and their structure is stabilized by grafting. They therefore exhibit high CO_2 capture performance and enhanced thermal stability during sorption and regeneration cycles compared with the sorbents prepared by the typical method (impregnation and grafting).

CONCLUSION

We have proposed a one-pot synthesis method for APTS-functionalized FS sorbents for CO_2 capture at low temperatures, where the synthesis process consists of (1) hydrolysis, (2) grafting, and (3) condensation steps. The APTS-functionalized FS sorbents had higher amine content that led to higher CO_2 capture capacity than typically prepared amine-grafted sorbents; they also demonstrated better thermal stability during the sorption (60 °C) and regeneration (120 °C) processes than typically prepared amine-impregnated sorbents. The optimum conditions were determined by testing parameters such as the APTS loading amount, sorption temperature, CO_2 concentration, and water vapor concentration. Among the amine-functionalized FS sorbents, the FS-APTS60 sorbent demonstrated acceptable CO_2 capture capacity (66.1 mg CO_2/g sorbent) in the presence of 1 vol% CO_2 and 10 vol% H_2O at 60 °C. Moreover, the CTAB created an additional CO_2 pathway to the amine sites as well as suppressed the condensation of the amino groups on the surface of the silica support. Consequently, the surfactant-promoted sorbents (FS-APTS65-CTAB5) exhibited greater BET surface areas and greater numbers of reactive amine sites, which improved the CO_2 capture capacity (83.4 mg CO_2/g sorbent). In addition, the surfactant-promoted amine sorbents exhibited excellent regeneration property in a short series of sorption/desorption cycles. The amine-functionalized FS sorbents prepared via the one-pot syn-

thesis method could become feasible sorbents for CO_2 capture at low temperatures because they are easy to prepare and exhibit multicycle stability with a high CO_2 capture capacity.

ACKNOWLEDGEMENT

This work was supported by the Korea Institute of Energy Technology Evaluation and Planning (KETEP) and the Ministry of Trade, Industry & Energy (MOTIE) of the Republic of Korea (No. 20182010600530).

SUPPORTING INFORMATION

Additional information as noted in the text. This information is available via the Internet at http://www.springer.com/chemistry/journal/11814.

REFERENCES

1. D. Aaron and C. Tsouris, *Sep. Sci. Technol.*, **40**, 321 (2005).
2. D. J. Hofmann, J. H. Butler and P. P. Tans, *Atmos. Environ.*, **43**, 2084 (2009).
3. D. W. Keith, *Science*, **325**, 1654 (2009).
4. L. V. Alexander, X. Zhang, T. C. Peterson, J. Caesar, B. Gleason, A. M. G. Klein Tank, M. Haylock, D. Collins, B. Trewin, F. Rahimzadeh, A. Tagipour, K. Rupa Kumar, J. Revadekar, G. Griffiths, L. Vincent, D. B. Stephenson, J. Burn, E. Aguilar, M. Brunet, M. Taylor, M. New, P. Zhai, M. Rusticucci and J. L. Vazquez-Aguirre, *J. Geophys. Res. Atmos.*, **111**, D05109 (2006).
5. N. P. Gillett, V. K. Arora, G. M. Flato, J. F. Scinocca and K. von Salzen, *Geophys. Res. Lett.*, **39**, L01704 (2012).
6. B. D. Santer, J. F. Painter, C. A. Mears, C. Doutriaux, P. Caldwell, J. M. Arblaster, P. J. Cameron-Smith, N. P. Gillett, P. J. Gleckler, J. Lanzante, J. Perlwitz, S. Solomon, P. A. Stott, K. E. Taylor, L. Terray, P. W. Thorne, M. F. Wehner, F. J. Wentz, T. M. L. Wigley, L. J. Wilcox and C.-Z. Zou, *Proc. Natl. Acad. Sci. U.S.A.*, **110**, 26 (2013).
7. T. R. Anderson, E. Hawkins and P. D. Jones, *Endeavour*, **40**, 178 (2016).
8. E. W. Maibach, J. M. Kreslake, C. Roser-Renouf, S. Rosenthal, G. Feinberg and A. A. Leiserowitz, *Ann. Global Health*, **81**, 396 (2015).
9. J. M. Melillo, T. Richmond and G. Yohe, *Third National Climate Assessment, U.S. Global Change Research Program* (2014).
10. J. L. Schnell, M. J. Prather, B. Josse, V. Naik, L. W. Horowitz, G. Zeng, D. T. Shindell and G. Faluvegi, *Geophys. Res. Lett.*, **43**, 3509 (2016).
11. D. P. Hagewiesche, S. S. Ashour, H. A. Al-Ghawas and O. C. Sandall, *Chem. Eng. Sci.*, **50**, 1071 (1995).
12. M. Mavroudi, S. Kaldis and G. Sakellaropoulos, *Fuel*, **82**, 2153 (2003).
13. A. Sayari, Y. Belmabkhout and R. Serna-Guerrero, *Chem. Eng. J.*, **171**, 760 (2011).
14. G. Sethia and A. Sayari, *Carbon*, **93**, 68 (2015).
15. C. Shen, C. A. Grande, P. Li, J. Yu and A. E. Rodrigues, *Chem. Eng. J.*, **160**, 398 (2010).
16. R. V. Siriwardane, M.-S. Shen, E. P. Fisher and J. A. Poston, *Energy Fuels*, **15**, 279 (2001).
17. Y. Takamura, S. Narita, J. Aoki, S. Hironaka and S. Uchida, *Sep. Purif. Technol.*, **24**, 519 (2001).
18. J. A. Thompson, J. T. Vaughn, N. A. Brunelli, W. J. Koros, C. W. Jones and S. Nair, *Micropor. Mesopor. Mater.*, **192**, 43 (2014).
19. Z. Yong, V. Mata and A. E. Rodrigues, *J. Chem. Eng. Data*, **45**, 1093 (2000).
20. Z. Yong, V. Mata and A. E. Rodrigues, *Ind. Eng. Chem. Res.*, **40**, 204 (2001).
21. Z. Yong, V. Mata and A. R. E. Rodrigues, *Sep. Purif. Technol.*, **26**, 195 (2002).
22. Z. Yong, V. G. Mata and A. E. Rodrigues, *Adsorption*, **7**, 41 (2001).
23. Z. Yong and A. R. E. Rodrigues, *Energy Convers. Manage.*, **43**, 1865 (2002).
24. Y. Zou and A. E. Rodrigues, *Ads. Sci. Technol.*, **19**, 255 (2001).
25. C. Chen, S.-T. Yang, W.-S. Ahn and R. Ryoo, *Chem. Commun.*, **24**, 3627 (2009).
26. A. Goeppert, S. Meth, G. S. Prakash and G. A. Olah, *Energy Environ. Sci.*, **3**, 1949 (2010).
27. G. Qi, Y. Wang, L. Estevez, A. K. Switzer, X. Duan, X. Yang and E. P. Giannelis, *Chem. Mater.*, **22**, 2693 (2010).
28. J. Wang, D. Long, H. Zhou, Q. Chen, X. Liu and L. Ling, *Energy Environ. Sci.*, **5**, 5742 (2012).
29. X. Xu, C. Song, J. M. Andresen, B. G. Miller and A. W. Scaroni, *Energy Fuels*, **16**, 1463 (2002).
30. X. Xu, C. Song, B. G. Miller and A. W. Scaroni, *Ind. Eng. Chem. Res.*, **44**, 8113 (2005).
31. A. C. Chang, S. S. Chuang, M. Gray and Y. Soong, *Energy Fuels*, **17**, 468 (2003).
32. S. W. Delaney, G. P. Knowles and A. L. Chaffee, *Fuel Chem. Div. Preprints*, **47**, 65 (2002).
33. M. W. Hahn, M. Steib, A. Jentys and J. A. Lercher, *J. Phys. Chem. C*, **119**, 4126 (2015).
34. P. J. Harlick and A. Sayari, *Ind. Eng. Chem. Res.*, **45**, 3248 (2006).
35. P. J. Harlick and A. Sayari, *Ind. Eng. Chem. Res.*, **46**, 446 (2007).
36. G. P. Knowles, S. W. Delaney and A. L. Chaffee, *Ind. Eng. Chem. Res.*, **45**, 2626 (2006).
37. O. Leal, C. Bolívar, C. Ovalles, J. J. García and Y. Espidel, *Inorg. Chim. Acta*, **240**, 183 (1995).
38. C. Chen, J. Kim and W.-S. Ahn, *Korean J. Chem. Eng.*, **31**, 1919 (2014).
39. J. Wang, L. Huang, R. Yang, Z. Zhang, J. Wu, Y. Gao, Q. Wang, D. O'Hare and Z. Zhong, *Energy Environ. Sci.*, **7**, 3478 (2014).
40. W. Choi, K. Min, C. Kim, Y. S. Ko, J. W. Jeon, H. Seo, Y.-K. Park and M. Choi, *Nat. Commun.*, **7**, 12640 (2016).
41. D. V. Quang, T. A. Hatton and M. R. Abu-Zahra, *Ind. Eng. Chem. Res.*, **55**, 7842 (2016).
42. I. Rahman, M. Jafarzadeh and C. Sipaut, *Ceram. Int.*, **35**, 1883 (2009).
43. K. S. Sing, *J. Porous Mater.*, **2**, 5 (1995).
44. N. Mittal, A. Samanta, P. Sarkar and R. Gupta, *Energy Sci. Eng.*, **3**, 207 (2015).
45. H.-J. Kim, W. Chaikittisilp, K.-S. Jang, S. A. Didas, J. R. Johnson, W. J. Koros, S. Nair and C. W. Jones, *Ind. Eng. Chem. Res.*, **54**, 4407 (2014).

Supporting Information

Thermally stable amine-functionalized silica sorbents using one-pot synthesis method for CO_2 capture at low temperature

Seong Bin Jo*, Ho Jin Chae*, Tae Young Kim, Jeom-In Baek***, Dhanusuraman Ragupathy****, Soo Chool Lee*,†, and Jae Chang Kim**,†**

*Research Institute of Advanced Energy Technology, Kyungpook National University, Daegu 41566, Korea
**Department of Chemical Engineering, Kyungpook National University, Daegu 41566, Korea
***Korea Electric Power Research Institute, Daejeon 34056, Korea
****Department of Chemistry, National Institute of Technology Puducherry, Karaikal 609609, India
(*Received 18 June 2020 • Revised 4 August 2020 • Accepted 4 August 2020*)

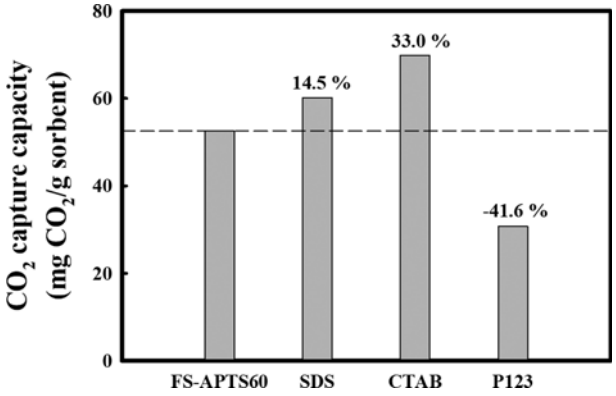

Fig. S1. CO_2 capture capacity of FS-APTS60 and surfactant-promoted sorbents loaded 60 wt% APTS with 5 wt% of different surfactants (SDS, CTAB, and P123) in the presence of 1 vol% CO_2 at 60 °C.

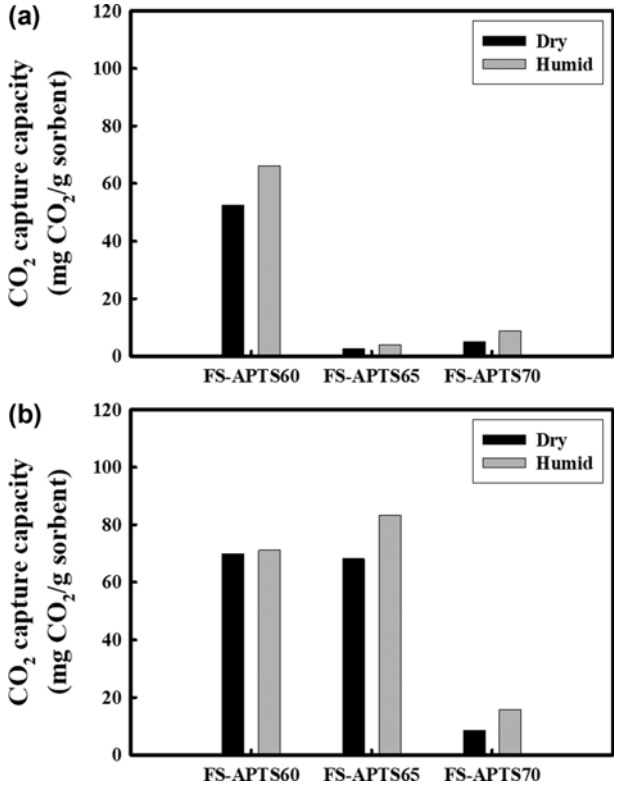

Fig. S2. CO_2 capture capacity of FS-APTS60, FS-APTS65, and FS-APTS70 (a) without and (b) with CTAB, in the presence of 1 vol% CO_2 at 60 °C.

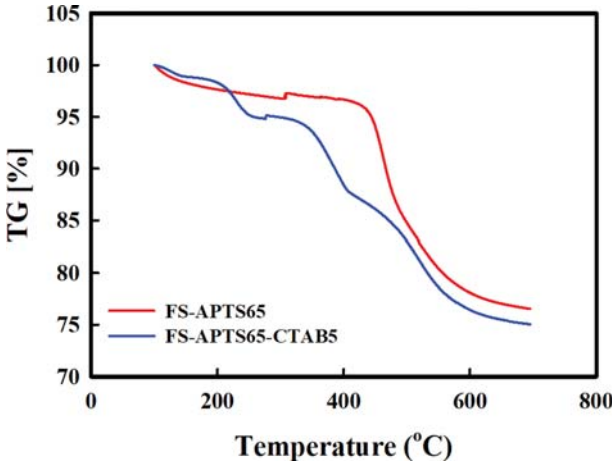

Fig. S3. TGA results of FS-APTS65 and FS-APTS65-CTAB5 sorbents.